Deeply penetrating in vivo photoacoustic imaging using a clinical ultrasound array system

Chulhong Kim,[1,3] Todd N. Erpelding,[2,3] Ladislav Jankovic,[2] Michael D. Pashley,[2] and Lihong V. Wang[1,*]

[1]*Optical Imaging Laboratory, Department of Biomedical Engineering, Washington University in St. Louis, Campus Box 1097, One Brookings Dr. St. Louis, MO 63130-4899, USA*
[2]*Philips Research North America, 345 Scarborough Rd. Briarcliff Manor, NY 10510, USA*
[3]*These authors contributed equally to this work.*
[*]lhwang@biomed.wustl.edu

Abstract: Using a hand-held photoacoustic probe integrated with a clinical ultrasound array system, we successfully imaged objects deeply positioned in biological tissues. The optical contrasts were enhanced by methylene blue with a concentration of ~30 mM. The penetration depth reached ~5.2 cm in chicken breast tissue by using 650-nm wavelength, which is ~4.7 times the $1/e$ optical penetration depth. This imaging depth was achieved using a laser fluence on the tissue surface of only 3 mJ/cm^2, which is 1/7 of the American National Standards Institute (ANSI) safety limit (20 mJ/cm^2). The noise equivalent sensitivity at this depth was ~11 mM. Further, after intradermal injection of methylene blue in a rat, a sentinel lymph node was easily detected *in vivo*, beneath a 2-cm thick layer of chicken breast. Also, blood located 3.5 cm deep in the rat was clearly imaged with intrinsic contrast. We have photoacoustically guided insertion of a needle into a rat sentinel lymph node with accumulated methylene blue. These results highlight the clinical potential of photoacoustic image-guided identification and needle biopsy of sentinel lymph nodes for axillary staging in breast cancer patients.

©2010 Optical Society of America

OCIS codes: (110.0110) Imaging systems; (170.0170) Medical optics and biotechnology; (170.5120) Photoacoustic imaging.

References and links

1. L. V. Wang, "Multiscale photoacoustic microscopy and computed tomography," Nat. Photonics **3**(9), 503–509 (2009).
2. S. Nie, D. T. Chiu, and R. N. Zare, "Probing individual molecules with confocal fluorescence microscopy," Science **266**(5187), 1018–1021 (1994).
3. W. Denk, J. H. Strickler, and W. W. Webb, "Two-photon laser scanning fluorescence microscopy," Science **248**(4951), 73–76 (1990).
4. D. Huang, E. A. Swanson, C. P. Lin, J. S. Schuman, W. G. Stinson, W. Chang, M. R. Hee, T. Flotte, K. Gregory, C. A. Puliafito, and et, "Optical coherence tomography," Science **254**(5035), 1178–1181 (1991).
5. B. W. Zeff, B. R. White, H. Dehghani, B. L. Schlaggar, and J. P. Culver, "Retinotopic mapping of adult human visual cortex with high-density diffuse optical tomography," Proc. Natl. Acad. Sci. U.S.A. **104**(29), 12169–12174 (2007).
6. C. Kim, C. Favazza, and L. V. Wang, "In vivo photoacoustic tomography of chemicals: high-resolution functional and molecular optical imaging at new depths," Chem. Rev. **110**(5), 2756–2782 (2010).
7. R. O. Esenaliev, A. A. Karabutov, and A. A. Oraevsky, "Sensitivity of laser opto-acoustic imaging in detection of small deeply embedded tumors," IEEE J. Sel. Top. Quantum Electron. **5**(4), 981–988 (1999).
8. G. Ku, and L. V. Wang, "Deeply penetrating photoacoustic tomography in biological tissues enhanced with an optical contrast agent," Opt. Lett. **30**(5), 507–509 (2005).
9. J. J. Albertini, G. H. Lyman, C. Cox, T. Yeatman, L. Balducci, N. Ku, S. Shivers, C. Berman, K. Wells, D. Rapaport, A. Shons, J. Horton, H. Greenberg, S. Nicosia, R. Clark, A. Cantor, and D. S. Reintgen, "Lymphatic mapping and sentinel node biopsy in the patient with breast cancer," JAMA **276**(22), 1818–1822 (1996).
10. A. E. Giuliano, D. M. Kirgan, J. M. Guenther, and D. L. Morton, "Lymphatic mapping and sentinel lymphadenectomy for breast cancer," Ann. Surg. **220**(3), 391–401 (1994).
11. D. N. Krag, D. L. Weaver, J. C. Alex, and J. T. Fairbank, "Surgical resection and radiolocalization of the sentinel lymph node in breast cancer using a gamma probe," Surg. Oncol. **2**(6), 335–340 (1993).

12. C. Kim, K. H. Song, F. Gao, and L. V. Wang, "Sentinel lymph nodes and lymphatic vessels: noninvasive dual-modality in vivo mapping by using indocyanine green in rats--volumetric spectroscopic photoacoustic imaging and planar fluorescence imaging," Radiology **255**(2), 442–450 (2010).
13. K. H. Song, C. Kim, C. M. Cobley, Y. Xia, and L. V. Wang, "Near-infrared gold nanocages as a new class of tracers for photoacoustic sentinel lymph node mapping on a rat model," Nano Lett. **9**(1), 183–188 (2009).
14. K. H. Song, E. W. Stein, J. A. Margenthaler, and L. V. Wang, "Noninvasive photoacoustic identification of sentinel lymph nodes containing methylene blue in vivo in a rat model," J. Biomed. Opt. **13**(5), 054033 (2008).
15. T. N. Erpelding, C. Kim, M. Pramanik, L. Jankovic, K. Maslov, Z. Guo, J. A. Margenthaler, M. D. Pashley, and L. V. Wang, "Sentinel lymph nodes in the rat: noninvasive photoacoustic and US imaging with a clinical US system," Radiology **256**(1), 102–110 (2010).
16. M. P. Fronheiser, S. A. Ermilov, H. P. Brecht, A. Conjusteau, R. Su, K. Mehta, and A. A. Oraevsky, "Real-time optoacoustic monitoring and three-dimensional mapping of a human arm vasculature," J. Biomed. Opt. **15**(2), 021305 (2010).
17. C. Kim, T. N. Erpelding, K. Maslov, L. Jankovic, W. J. Akers, L. Song, S. Achilefu, J. A. Margenthaler, M. D. Pashley, and L. V. Wang, "Hand-held array-based photoacoustic probe for guiding needle biopsy of sentinel lymph nodes," J. Biomed. Opt. In press.
18. J. Su, A. Karpiouk, B. Wang, and S. Emelianov, "Photoacoustic imaging of clinical metal needles in tissue," J. Biomed. Opt. **15**(2), 021309 (2010).
19. "American national standard for the safe use of lasers," (ANSI. Inc., New York, 2002), pp. Standard Z136.131–2000.
20. K. P. Köstli, M. Frenz, H. Bebie, and H. P. Weber, "Temporal backward projection of optoacoustic pressure transients using fourier transform methods," Phys. Med. Biol. **46**(7), 1863–1872 (2001).
21. Y. Masannat, H. Shenoy, V. Speirs, A. Hanby, and K. Horgan, "Properties and characteristics of the dyes injected to assist axillary sentinel node localization in breast surgery," Eur. J. Surg. Oncol. **32**(4), 381–384 (2006).
22. G. Marquez, L. V. Wang, S. P. Lin, J. A. Schwartz, and S. L. Thomsen, "Anisotropy in the absorption and scattering spectra of chicken breast tissue," Appl. Opt. **37**(4), 798–804 (1998).
23. L. Spinelli, A. Torricelli, A. Pifferi, P. Taroni, G. M. Danesini, and R. Cubeddu, "Bulk optical properties and tissue components in the female breast from multiwavelength time-resolved optical mammography," J. Biomed. Opt. **9**(6), 1137–1142 (2004).
24. Z. Guo, L. Li, and L. V. Wang, "On the speckle-free nature of photoacoustic tomography," Med. Phys. **36**(9), 4084–4088 (2009).

1. Introduction

Optical imaging [1] has received great attention in biomedicine because of its rich contrast and nonionizing radiation. However, due to strong light scattering, pure optical imaging modalities suffer from either shallow penetration depth (e.g., confocal microscopy [2], two-photon microscopy [3], and optical coherence tomography [4]) or poor spatial resolution (e.g., diffuse optical tomography (DOT) [5]). The maximum penetration depth of optical microscopy using ballistic or quasi-ballistic photons is typically limited to one optical transport mean free path (~1 mm). Using diffusive photons, DOT with model-based reconstruction is able to provide both optical scattering and absorption parameters, so the penetration depth is extended to a few centimeters. However, this technique struggles with poor spatial resolution, typically 1/5 of the imaging depth. This fundamental issue of light diffusion has hindered pure optical imaging techniques from achieving widespread clinical application.

Photoacoustic (PA) imaging [1,6] has overcome the drawback of pure optical imaging by taking advantage of rich optical contrast and ultrasonic spatial resolution for deep imaging. It is capable of high-resolution structural, functional, and molecular imaging free from speckle artifacts. More importantly, because of its ultrasonic detection mechanism, the penetration depth and spatial resolution are scalable even beyond the optical transport mean free path in optically scattering media. Centimeter-scale imaging depths have been achieved. Oraevsky *et al.* demonstrated PA imaging in tissue mimicking phantoms and biological tissues at penetration depths exceeding 5 cm [7]. By enhancing the optical contrast with indocyanine green, Ku *et al.* photoacoustically imaged objects embedded at depths of greater than 5 cm in biological tissues [8].

Recently, PA imaging has been proposed as a noninvasive method of identifying sentinel lymph nodes and guiding fine needle aspiration or core needle biopsies. Sentinel lymph node biopsy (SLNB) is the emerging standard for axillary lymph node staging in clinically node-negative breast cancer patients [9–11]. Axillary staging is critical in planning appropriate

treatment and estimating patient prognosis. The current SLNB technique requires injection of blue dyes and/or radioactive tracers, followed by surgical removal of sentinel nodes for pathological examination. Compared with the current surgical SLNB, the photoacoustically guided minimally invasive approach has the potential to significantly reduce the impact on patients. Song *et al.* imaged *in vivo* deeply positioned (>3 cm) rat sentinel lymph nodes (SLNs) stained with either methylene blue or gold nanocages [12–14]. We have previously reported *in vivo* PA and ultrasound (US) mapping of SLNs in rats using a clinical US array [15]. An US probe combined with a fiber-based light delivery system enabled hand-held scanning analogous to ultrasonography [16,17]. Further, this hand-held probe enabled photoacoustic image-guided needle insertion [17,18]. Combined US and PA imaging systems provide US imaging for locating lymph nodes and PA imaging for identifying which nodes are sentinel based on the accumulation of blue dye. US imaging alone cannot identify which lymph nodes are sentinel nodes.

In this paper, we demonstrate deeply penetrating PA imaging using a hand-held PA/US probe with a modified clinical US array system. We successfully imaged a tube filled with methylene blue (~30 mM) at a depth of 5.2 cm in chicken breast tissues. This imaging depth was achieved using a light fluence on the tissue surface of only 3 mJ/cm^2, 1/7 of the ANSI safety limit [19]. Further, we report noninvasive *in vivo* imaging of deeply positioned (~2 cm) methylene-blue-dyed SLNs and metal needles in rats.

2. Methods and Materials

Figure 1 is a photograph of the integrated PA and US imaging system, modified from a clinical US array system (iU22, Philips Healthcare) [15]. The original channel board architecture of the US imaging system was modified to acquire raw per-channel PA and US data. Raw data was transferred to a data acquisition (DAQ) computer where post-processing was performed. The DAQ system controlled the laser firing and optical-wavelength tuning. PA images were processed using Fourier beam forming reconstruction [20], and displayed at ~1 fps. Yet, the maximum data acquisition rate is 10 fps, limited by the current laser repetition rate. A linear array US probe with a nominal bandwidth of 4-8 MHz (L8-4, Philips Healthcare) was physically integrated with a bifurcated optical fiber bundle (CB18043, Fiberguide), forming a hand-held probe. A zoomed-in photograph of the hand-held probe is shown in Fig. 1. Laser pulses with a 6.5-ns pulse duration and 10-Hz repetition rate were generated from a tunable dye laser (NS, Sirah) pumped by a Q-switched Nd:YAG laser (PRO-350-10, Newport). An optical wavelength of 650 nm, close to the peak optical absorption wavelength of methylene blue (667 nm), was utilized. Light fluence on the skin was ~3 mJ/cm^2 (total energy, 36 mJ; illumination area, ~12 cm^2), well below the ANSI safety limit (20 mJ/cm^2). We directly coupled the hand-held probe to tissue surfaces via US coupling gel.

We increased the imaging depth by stacking layers of chicken breast tissue. An optically transparent plastic tube (7 mm in diameter × 25 mm in length) filled with ~30-mM methylene blue was embedded in chicken breast tissue. The position of the tube was confirmed using US imaging. Here, the hand-held probe was mechanically fixed to avoid motion artifacts.

Institutional animal care and use committee approval (Washington University in St. Louis) was obtained. Sprague Dawley rats (~200 g) were initially anesthetized using a mixture of Ketamine (80 mg/kg) and Xylazine (8 mg/kg). For *in vivo* imaging, we also intentionally increased the imaging depth by placing ~2 cm thick chicken tissue atop the rat. After hair removal in the left axillary region of the rats, we acquired a control PA image before the injection of methylene blue. After intradermal injection of 0.1 ml of methylene blue (30 mM) into the left forepaw, a series of PA images were obtained to detect the methylene blue in the SLN. Many surgeons prefer methylene blue over isosulfan blue (the only FDA-approved dye for axillary SLNB) for SLNB as it is readily available, cost-effective, and anaphylaxis is rare [21]. Normal lymph nodes do not significantly absorb light at 650 nm, so only lymph nodes containing methylene blue are visible in PA images. Then, we photoacoustically tracked the insertion of a metal needle (18 gauge or 1.27 mm in diameter) *in vivo*. After all *in vivo* experiments, we visually confirmed the uptake of methylene blue in the excised lymph nodes.
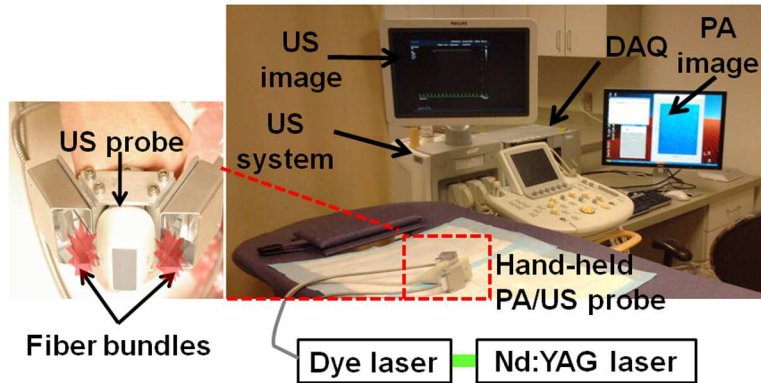
Fig. 1. Photograph of an integrated photoacoustic (PA) and ultrasound (US) imaging system modified from a clinical US array system.

3. Results and Discussion

A transparent plastic tube filled with methylene blue was embedded in chicken breast tissues (Fig. 2a). The imaging depth was incremented by overlaying chicken breast tissue (Fig. 2b). The top and bottom surfaces of the tube were positioned at depths of 4.5 and 5.2 cm from the tissue surface, respectively. To improve the signal-to-noise ratios (SNRs), we averaged the PA signals 100 times. The PA image clearly delineates the top and bottom boundaries of the tube (Fig. 2c). Figure 2d, created by overlaying the PA and US images, shows both the tube structure (US) and the methylene blue (PA) in the tube. The previously reported penetration depth for $1/e$ decay in chicken breast tissue is ~1.1 cm at an optical wavelength of 650 nm [22], where the $1/e$ penetration depth at 785 nm in human breast measured ~0.89 cm [23]. Therefore, the 5.2-cm imaging depth is equivalent to ~4.7 times the $1/e$ optical penetration depth, corresponding to a 20-dB attenuation from the surface. Table 1 summaries the PA experimental results acquired from the top and bottom surfaces of the tube, including SNR, image contrast, noise equivalent sensitivity (NES), and axial resolution. The SNR was defined as the mean of PA signals obtained from the tube divided by the standard deviation of the background signals. The background signals were selected from adjacent regions at the same depth of the tube. The image contrast was defined as the ratio of the difference between the average PA signal measured from the tube and the average background signal to the average background signal. The NES was defined as the ratio of the concentration of methylene blue to the SNR. The axial resolution was calculated with the full width at half maximum (FWHM) of the 1D profile taken across each of the two tube boundaries. At the 5.2-cm deep bottom boundary, the SNR was ~2.7, the image contrast was ~60%, and the NES was ~11 mM. Because of the low SNR at this depth, it was difficult to estimate the axial resolution. The estimated axial resolution from the 1D profile acquired from the top boundary was ~400 μm, which was close to the theoretical axial resolution (~385 μm). Again, a laser fluence of only 3 mJ/cm^2 (1/7 ANSI safety limit) was used for these experiments. If the laser fluence is increased to 20 mJ/cm^2 (the ANSI safety limit), the penetration depth can theoretically be extended to ~7.4 cm.
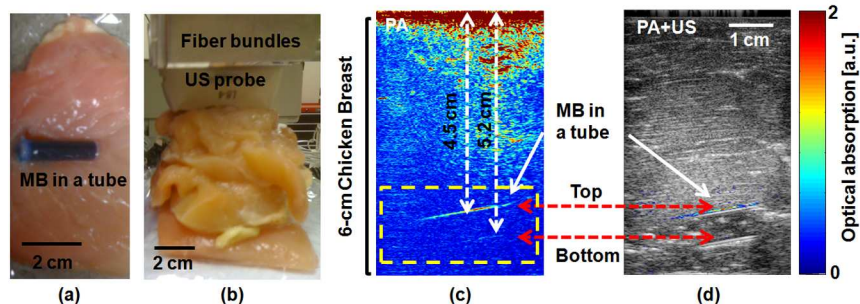
Fig. 2. Deeply penetrating PA imaging in biological tissues. Photographs of (a) the cross section of chicken breast tissue in which a transparent tube containing methylene blue (MB) is embedded and (b) the entire sample. (c) PA image of the tube containing MB. (d) Overlaid PA (pseudo color) and US (gray) image. The thresholded PA signals in the yellow dotted box in (c) were overlaid with the US image in (d).

Table 1. Experimental results of deeply penetrating PA imaging in biological tissues.

	Depth [cm]	SNR	Image contrast	NES[b] [mM]	FWHM [µm]
Top[a]	4.5	7.5	3.4	4	~400
Bottom[a]	5.2	2.7	0.6	11	N/A[c]

[a]Top and bottom denote the top and bottom boundaries of the tube.
[b]NES: Noise equivalent sensitivity.
[c]Due to low SNR, it was difficult to estimate the FWHM from the bottom surface of the tube.

To explore dual-modality PA and US mapping of deeply located SLNs (~2 cm) with methylene blue, we imaged the axillary region in a rat before and after methylene blue injection. Figure 3a shows a control PA B-scan image. Interestingly, two deeply positioned blood vessels at 3.2- and 3.5-cm depths are clearly seen in the control image with only intrinsic contrast. In addition, the posterior skin surface at a depth of 4.2 cm is clearly visible in the image as a result of unintentional staining with methylene blue. After methylene blue injection, the dye propagates through lymphatic vessels and accumulates in the sentinel node. We photoacoustically imaged the uptake of methylene blue in the SLN. Figure 3b shows the PA image of the methylene-blue-dyed SLN obtained at 10 minutes post-injection. The image contrast of the SLN enhanced by methylene blue accumulation was 14 ± 1.2. The overlaid PA and US images, as shown in Fig. 3c, provide both morphological information and functional information (i.e., methylene blue uptake in the SLN). Pseudo colors in Figs. 3a–3c shared the same dynamic range for comparison. The image SNR of the SLN stained with methylene blue at 2 cm is 21; those of two blood vessels at 3.2 and 3.5 cm are 18 and 14, respectively; and that of the skin stained with methylene blue at 4.2 cm is 11. No signal averaging has been applied to *in vivo* studies. The current imaging depths reached by this imaging system are compatible with the depths of axillary lymph nodes in humans (< ~3 cm), which highlights its potential clinical utility.
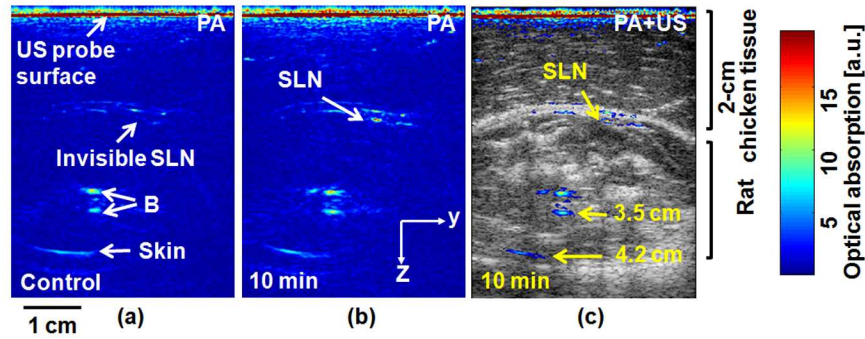
Fig. 3. *In vivo* deeply penetrating PA imaging. (a) Control PA image acquired before methylene blue injection. (b) PA image taken 10 minutes after methylene blue injection. (c) Overlaid post-injection PA (pseudo color) and US (gray scale) images. B, blood and SLN, sentinel lymph node.

As shown in Fig. 4, *in vivo* PA imaging simultaneously detected both the methylene blue uptake in the SLN and the inserted 18 gauge needle. Unlike ultrasonography, no speckle artifacts are visible in the PA image [24]. The image contrast of the biopsy needle at a depth of 1.7 cm was ~18.2 ± 1.0. US imaging has a limited angular sensitivity for detecting a needle, as most of the incident acoustic energy is reflected away from the limited aperture US probe. In comparison, generated PA waves are approximately cylindrical. As a result, PA imaging offers an improved angular sensitivity compared with conventional US imaging.
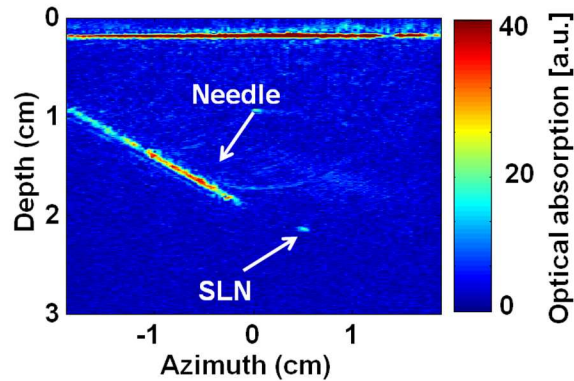

Fig. 4. *In vivo* PA guidance of a metal needle (18-gauge). SLN, sentinel lymph node.

4. Conclusions

We successfully imaged deeply positioned tubes (~5.2 cm) filled with methylene blue (~30 mM) in biological tissues, using a hand-held PA and US imaging system. The laser fluence on the tissue surface was only 1/7 of the ANSI safety limit. Deeply positioned rat blood (3.5 cm) was visible in the PA image with intrinsic contrast from hemoglobin. *In vivo* PA mapping of rat SLNs at an imaging depth of ~2 cm was accomplished following intradermal injection of methylene blue. Moreover, needle insertion was photoacoustically guided *in vivo* with high contrast. PA and US image-guided SLN identification and needle biopsy comprise a promising potential alternative to current invasive axillary staging methods for breast cancer patients.

Acknowledgement

financial interest in Microphotoacoustics, Inc. and in Endra, Inc., which, however, did not support this work.